

# IS THE BUTCHER-OEMLER EFFECT A FUNCTION OF THE CLUSTER REDSHIFT?

S. ANDREON

Osservatorio Astronomico di Capodimonte, via Moiariello 16, 80131 Napoli, Italy  
 E-mail: andreon@na.astro.it

AND

S. ETTORI

Institute of Astronomy, Madingley Road, Cambridge CB3 0HA, UK  
 E-mail: settori@ast.cam.ac.uk

*Submitted to The Astrophysical Journal*

## ABSTRACT

Using PSPC *Rosat* data, we measure x-ray surface brightness profiles, size and luminosity of the Butcher-Oemler (BO) sample of clusters of galaxies. The cluster x-ray size, as measured by the Petrosian  $r_{\eta=2}$  radius, does not change with redshift and is independent from x-ray luminosity. On the other hand, the x-ray luminosity increases with redshift. Considering that fair samples show no-evolution, or negative luminosity evolution, we conclude that the BO sample is not formed from the same class of objects observed at different look-back times. This is in conflict with the usual interpretation of the Butcher-Oemler as an evolutionary (or redshift-dependent) effect, based on the assumption that we are comparing the same class of objects at different redshifts. Other trends present in the BO sample reflect selection criteria rather than differences in look-back time, as independently confirmed by the fact that trends loose strength when we enlarge the sample with x-ray selected sample of clusters. The variety of optical sizes and shapes of the clusters in the Butcher-Oemler sample, and the Malmquist-like bias, are the reasons for these selection effects that mimic the trends usually interpreted as changes due to evolution.

*Subject headings:* Galaxies: evolution — galaxies: clusters: general — X-rays: general

## 1. INTRODUCTION

Galaxies in distant ( $z \sim 0.4$ ) clusters differ from those in the nearby systems (e.g. Butcher & Oemler 1984; Dressler & Gunn 1992). There is a blueing of galaxy color with redshift, also known as Butcher-Oemler effect (hereafter BO effect, Butcher & Oemler 1977, 1984). At  $z \sim 0.4$  there is a population of almost normal late-type galaxies that by the present epoch has disappeared, faded or has been disrupted (Dressler et al. 1997). Distant clusters contain galaxies with disturbed morphologies and peculiar spectra. The occurrence of these peculiarities varies from cluster to cluster and, on average, increases with redshift. In general, the change of galaxy properties is explained as the effect of some kind of evolution.

Oemler, Dressler & Butcher (1997) proposed a physical reason to explain why most of the clusters showing a BO effect are at high redshift and almost none at the present epoch: clusters at  $z \sim 0.4$  are much more exceptional objects than present-day clusters and they are observed in the act of growing by merger of smaller clumps, in agreement with a hierarchical growth of structures as described, for example, by Kauffmann (1995). Furthermore, this scenario permits the existence of dynamically young local clusters, such as the spiral rich Abell 1367 and 2151 clusters, and evolved clusters at high redshift, such as Cl 0024+16. In the Oemler et al. (1997) interpretation of the BO effect, clusters at higher redshift are dynamically younger, on average, than the nearby ones, because we are looking at the epoch of an enhanced cluster formation.

Allington-Smith et al. (1993) showed that galaxies in groups do not evolve (except passively) and suggest that the BO effect should be interpreted as an evidence of the

important role played by the cluster environment: evolution is strong in clusters and negligible in groups. However this idea have been questioned: Rakos & Schombert (1995) show that it is difficult to fade the majority of the cluster population at  $z \sim 0.7$  to make their blue population as scarce as in present-day clusters. Andreon, Davoust & Heim (1997) and Ellis et al. (1997) show that cluster ellipticals and lenticulars are old galaxies already at  $z \sim 0.4$ , and that the majority of them cannot be the end product of the blue galaxy population. Recently, this result has been extended with clusters up to  $z \sim 0.9$  (Stanford, Eisenhardt & Dickinson 1998).

Andreon et al. (1997) have made a detailed comparison of the properties of galaxies in the nearby Coma cluster and the distant cluster, Cl 0939+47. They found that the spiral population of these two clusters appears too different in spatial, color and surface brightness distributions to be the same galaxy population observed at two different epochs. The Coma cluster is therefore unlikely to be representative of the end of the evolution path of Cl 0939+47.

In order to quantify the effect of evolution on the properties of a given class of objects, it is required that the observed class is the same at different times. In the case of the evolution of galaxies in clusters, it is necessary that the high redshift clusters studied are the ancestors of the investigated present-day clusters.

The goal of this paper is to test whether the distant and nearby clusters of the BO sample are really the same population seen at different epochs or two different populations; in other words, we want to check if we are comparing unripe apples to ripe oranges in understanding how fruit ripens!. We achieve this goal by means of the X-ray

properties of the clusters of galaxies, whose evolution is known.

The paper is organized as follows: in the next section, we present our sample of clusters. In Section 3, we discuss the x-ray analysis of their images. The observed trends and their relevance on the BO effect are presented in Section 4 and 5, respectively. In Section 6, we summarize our main results.

In the following analysis, we adopt  $H_0 = 50 \text{ km s}^{-1} \text{ Mpc}^{-1}$  and  $q_0 = 0.5$ . The conversion to the physical dimension is done through the equation (Sandage 1988):

$$r(\text{kpc}) = 2.91 \cdot 10^3 \times \theta \frac{z+1-\sqrt{z+1}}{H_0 (1+z)^2}, \quad (1)$$

where  $\theta$  is the angular radius in arcsec.

## 2. OUR SAMPLE: THE BUTCHER & OEMLER (1985) SAMPLE

The clusters most frequently compared for measuring the BO effect are listed in Butcher & Oemler (1985). This list is the master list for many studies (e.g. Dressler & Gunn 1992; Oemler, Dressler & Butcher 1997; half of the sample by Smail et al. 1997; Dressler et al. 1998 is drawn from the BO sample, etc.).

Our sample is made from the BO sample plus Cl 0939+47, a cluster at  $z \sim 0.4$  which is frequently studied in the context of the BO effect. This sample, which consist of 33(+1) clusters, is not complete in any sense (in cluster richness, in  $z$ , etc.). Figure 1 reproduces Figure 3 in Butcher & Oemler (1984), with the addition of Cl 0939+47. The BO effect is evident from the increase of the fraction of blue galaxies with the redshift.

We have x-ray data for 30 of the 34 clusters. Position Sensitive Proportional Counter (PSPC) images are available for 25 of these. We call this subsample ‘‘HQ’’ (high quality) sample. Five more clusters, as well as many of the clusters observed by *Rosat*, have been observed with previous x-ray missions. We use these old data when necessary.

Table 1 presents the whole sample in order of increasing redshift. A double tick and a single tick in the last column indicate that the cluster belongs to the HQ sample and we collect x-ray flux from literature, respectively. Columns 1, 2, 3, 4, 5 and 6 list respectively the cluster name, the cluster redshift, the radius  $r_{30}$  that contain 30 % of the whole cluster population, the number of galaxies  $N_{30}$  inside such a radius, and the cluster blue fraction  $f_b$  (from Butcher & Oemler (1985)). Columns 7 and 8 list the Galactic HI column (from Stark et al. 1992) toward the cluster direction and the cluster richness [from the Abell, Corwin & Olowin (1989, hereafter ACO) catalog]. We update the richness classification of the Cl 0939+47 (Abell 851) and Abell 370 clusters, and we attribute a richness to Cl 0024+16 by adopting the more accurate values listed in Oemler et al. (1997). Cl 0016+16 is twice as rich as Coma (Koo 1981). The ACO richness, according to its definition, is the background corrected number of galaxies within 3 Mpc from the cluster center having luminosity in the range  $M_3$  and  $M_3 + 2$ , where  $M_3$  is the magnitude of the third brightest cluster galaxy.

## 3. DATA ANALYSIS

### 3.1. Data reduction

PSPC images in the hard band 0.5–2 keV with 15 arcsec pixel size have been extracted from the public archive at the Max–Planck–Institut für extraterrestrische Physik (MPE) or at the Goddard Space Flight Center (according to their availability). Table 2 lists x-ray related quantities. We correct our images for exposure variation and telescope vignetting using the distributed exposure maps. All pixels contaminated by other objects or occulted by ribs have been flagged and excluded from the following analysis.

In order to measure the x-ray radial profiles, brightnesses are computed in elliptical annuli of semi-major axis increasing in geometrical progression of base  $\sqrt{2}$  in order to take the S/N approximatively constant along the radius.

Ellipticity, position angle (PA hereafter) and center for the cluster emission have been derived paying attention to the observational data available for distant clusters. For example, we keep fixed the center, even if isophotes center moves, since in distant clusters we seldom have data of good enough quality to measure the displacement of the center of the various isophotes. When data are not good enough to estimate the ellipticity or the position angle, we adopt circular apertures.

The details of the data reduction are as follows:

- The equivalent radius of each ellipse is that of a circle of the same area, i.e.  $r = \sqrt{ab}$ , where  $a, b$  are the major and minor axis of the ellipse.
- The axis lengths of an elliptical annulus of finite width are at half way from the internal and external edges.
- The brightness in an annulus is computed as the ratio of the intensity measured in unflagged pixels and their total area.
- We assume that flagged pixels have the same brightness as unflagged ones in the same annulus. The flux inside an ellipse is the sum, over the internal annulus, of the product of the brightness computed in each annulus and the total area of the annulus (calculated including the flagged pixels).

Before we proceed further in the data analysis we need to verify two assumptions: the computed profiles are independent of the exact choice of the flagged pixels and of the ellipticity and PA chosen for the integration. We apply two different flag schemes to the same image of Abell 2218: (i) we flag only superposed objects and ribs, (ii) we flags every small fluctuation, including very faint ones at the level of the noise. The resulting profiles are indistinguishable. Further confirmation of the independence of the exact choice of the pixels flagged came from the comparison of independent analysis of the same images (see next section).

In order to test the sensitivity of our profile to the chosen axis ratio, we compute the profiles of Abell 2218 within elliptical annuli of axis ratio 0.83 and 1. The two profiles are, again, indistinguishable. The profiles of some other clusters, taken from the literature, measured through ellipses of different shapes agree within the errors. Our elliptical profiles do not depend upon the adopted axis ratio, due to our selection of the axis length, and the fact that the PA and ellipticity of the x-ray isophotes are not subject to large variations.

Furthermore, we adjust the background level of the Abell 1656 cluster, the emission of which almost fills the PSPC field of view, in such a way that our profile at large radii matches those derived in literature from the *Rosat* All Sky Survey images (Briel, Henry & Boeringer 1992). Abell 400 exhibits a central point source, a dumbbell galaxy also known as radio source 3C75, with a slight offset with respect to the center of the cluster emission (cf. Beers et al. 1992). Pixels affected by this source have been flagged. Some other clusters in our list have some peculiar features in their x-ray profile: Abell 1689, 2199 and 2634 present a strong cooling flow (Allen & Fabian 1998, White et al. 1997 and Schindler & Prieto 1996, respectively). In the following figures, we represent with squares symbols these cooling flows clusters.

### 3.2. Comparisons with previous *Rosat* data

A comparison between our profiles and those from literature is quite difficult. For most of the clusters, the data points of the surface brightness profile are not available. Generally, the best-fit parameters for a  $\beta$ -model (Cavaliere & Fusco-Femiano 1976) are the only quantities quoted. We will use these for our comparisons, even if some information is still missing, such as (i) the adopted center, ellipticity and position angle (for elliptical profiles), (ii) the value of the central brightness, (iii) the radius up to which the data are fitted, (iv) how well the model describes the profile, in terms of the location of the deviations from the best fit. Finally some literature values are wrong through mistake or typographical errors.

Figure 2 shows good agreement between the best fits as obtained from literature, once the necessary (if any) corrections were introduced, and our profiles. Here we note that where we see a local mismatch between the data and the best fit, the same deviations are often observed in the published surface brightness profile.

#### 3.2.1. Remarks on individual clusters

Abell 262: David, Jones, & Forman (1996) found that the x-ray isophotes of this cluster twist and ellipticity changes with radius. They present a detailed analysis of the x-ray profile computed through elliptical apertures whose PA and ellipticity are fitted to the cluster isophotes. However, they list only counts integrated within ellipses of unspecified PA and ellipticity, both of which are probably changing with radius. In our comparison, to compute the surface brightness profile, we calculate the gradient of the integrated flux in each ellipse and make the approximation that it was computed within ellipses with the same centre and axis ratio of 0.8. Our profile matches exactly the one from literature at  $\log(r) > 2.4$ . The agreement is satisfactory at smaller radii given the approximation involved in the comparison.

Abell 401: Our points match well those of Buote & Canizares (1996)  $\beta$  model. Another observation performed 6 months later is in good agreement with the plotted profile, confirming also the temporal stability of the *Rosat* PSPC.

Abell 1656: Our points lie on the best-fit  $\beta$  models in Buote & Canizares (1996) and Briel, Henry & Boeringer (1992).

Abell 2199: This has been observed twice with a temporal gap of 3 years. As for A401, the two profiles are in good agreement between them and with Buote & Canizares (1996)  $\beta$  model.

Abell 2256: This is a quite studied merging cluster (Markevitch & Vikhlinin 1997, Buote & Canizares 1996; Briel, Henry & Boeringer 1992). Our center is not located on the peak emission but on the barycenter of the x-ray emission. This explains the rising profile at small radii and the slight differences with the fit functions from literature.

Abell 2634: This cluster presents a strong cooling flow, and is not described at all by a  $\beta$  model for  $\log(r) < 2.4$ . At larger radii, where the profile matches the  $\beta$  model, our data are consistent with the best-fit  $\beta$  model in Schindler & Prieto (1996).

Cl0939+4713: Our profile agrees well with the Schindler & Wambsganss (1996)  $\beta$  profile.

### 3.3. Characterization of the cluster profiles

Usually x-ray profiles are characterized through some parameters, resulting from a fit to the data of an appropriate function, generally a  $\beta$  model. The use of this model presents some problems. Firstly, this method is parametric and introduces the width of the bin in the extracted profile as no-physical scale. Secondly, the  $\beta$  parameter, often referred to as the ‘slope’, is not properly the slope of the profile at large radii, as one can verify calculating the radial gradient of the  $\beta$  model or, more simply, plotting two profiles with the same  $\beta$ , but different core radii. Thirdly, the best-fit parameters are generally a function of the amplitude of the errors.

For these reasons, we prefer to characterize cluster x-ray profiles through a no-parametric way, computing Petrosian (1976) quantities. A detailed and recent presentation of Petrosian quantities can be found in Sandage & Perlmutter (1990). Briefly, the Petrosian radius  $r_\eta$  is defined as the radius where the surface brightness *at* that radius is  $\eta$  times fainter than the surface brightness *inside* that radius. Figure 3 shows the surface brightness ( $SB(r)$ ) and the  $\eta(r)$  profiles for a King profile, where  $\eta(r) = SB(< r)/SB(r)$ .

Choosing a value for  $\eta$ , of say 2, the corresponding radius  $r_{\eta=2}$  is completely determined (in our example  $\log(r) \sim 2.8$ ). The Petrosian radius, as a ratio between two surface brightnesses, does not depend from quantities that usually affect surface brightnesses, such as Galactic absorption, cosmological dimming, K-correction and even luminosity evolution if it is the same at all radii. It could be shown (Petrosian 1976), that the Petrosian radius is a metric radius, i.e. its angular dimension is given by the formula relating the physical dimension of a rigid rod and its angular dimension. For objects with profiles of the same shape, the luminosity within a fixed Petrosian radius gives a fixed fraction of the total luminosity, as the effective radius for the de Vaucouleurs’ (1976) law. We choose  $2.5 \log \eta = 2$ , and we refer to it as “ $\eta = 2$ ”. For Hubble and  $\beta$  model (with  $\beta = 2/3$ ) profiles,  $\eta = 2$  correspond to 55 and 38 core radii, respectively.

### 3.4. Luminosities & errors

The count rates have been converted to the flux in the 0.5-2 keV band using a conversion factor of  $1.15 \times 10^{-11}$

$\text{erg s}^{-1} \text{ cm}^{-2} / (\text{count s}^{-1})$ , almost independent from the gas temperature. The correction for the Galactic absorption has been calculated applying the Morrison & McCammon (1983) model as a foreground absorber to the thermal emission from the intracluster plasma with metallicity fixed to 0.3 (Raymond, & Smith 1977; up to date version 1992 in XSPEC version 10). Since all clusters are at high Galactic latitude, this correction is small. K-corrections have been computed individually assuming thermal cluster spectrum. Temperatures have been taken from White, Jones & Forman (1997). For the clusters Abell 222, 223, 777, 963, 1758, 1904, 2125, and Cl 0024+16, Cl 0939+47, that are not listed in White et al. 1997, we adopt a temperature of 4 keV. Our K-corrections are compatible with the more accurate values plotted by Jones et al. (1998) in their Figure 7. Differences amount to 0.01 in  $\log(L_X)$  at most, i.e. are negligible.

Our estimate of the uncertainties include Poisson errors and a generous 10% error on the determination of the background level. In Figure 4, and subsequent plots, we do not plot the errors on the x-ray flux, since they are smaller than the symbol size, except for two clusters (Abell 777 and Cl0024, whose fluxes are lower limits).

### 3.5. Comparison with data from previous x-ray missions

For the clusters of our sample, the x-ray luminosities measured by previous missions are listed in various compilations (Salten & Henry 1983; Lea & Henry 1988; Mushotzky & Scharf 1997; Sadat, Blanchard, Guiderdoni & Silk 1998). Their luminosities are not measured at the Petrosian radii, nor in the *Rosat* hard band, but are simply aperture or isophotal fluxes, usually in the band of observation. We convert them in our system (flux measured in the Petrosian  $r_{\eta=2}$  radius in *Rosat* hard band) empirically, by means of the median difference between the (log of the) luminosities in common clusters. Our fluxes correlate well with literature ones transformed in our system, as shown in Figure 4. The large scatter is due to the heterogeneity of literature data and to the transformation from one band to another, since the formal error on the x-ray flux in our system is smaller than the point size. The two outliers refer to the cluster Abell 400, whose central emission has been masked out in our flux measure (see Section 3.2.1), but not in the two estimates from literature.

## 4. RESULTS: THE TRENDS

The aim of this section is to show the existence of trends between quantities related to clusters properties (richness, size, distance, x-ray flux, etc.), and to understand the role played by selection effects on these trends.

### 4.1. Size

Table 3 quotes the  $r_{\eta=2}$  size of the HQ sample. All clusters, spanning a large redshift range, from  $z \sim 0$  to  $z \sim 0.6$ , have similar sizes of  $\log r \sim 3.10$  kpc with a scatter (in  $\log r$ ) of only 0.14 (see Figure 5). The outliers (at small  $r_{\eta=2}$ ) appear to be cooling flow clusters. Cl 0024+16 and Abell 777 have a too noisy profile to compute  $r_{\eta=2}$ . Our results confirm those obtained from Henry et al. (1979) and Vikhlinin et al. (1998). Figure 6 shows

that clusters have similar size, independently on their x-ray luminosity, at least in the luminosity range sampled ( $43.5 < \log L_X < 45.5 \text{ erg s}^{-1}$ ). Furthermore clusters rich in blue galaxies (solid dots in the figure) are not preferentially larger, smaller, brighter or fainter than those clusters poor in blue galaxies.

Figure 7 compares the optical cluster radius, defined as the radius which encloses 30 % of the galaxy population,  $r_{30}$ , with our x-ray  $r_{\eta=2}$  size, for the HQ sample. The  $r_{\eta=2}$  is in average  $\sim 3$  times larger than  $r_{30}$ , with a large scatter. Clusters rich in blue galaxies (solid dots) do not have systematically larger or smaller  $r_{\eta=2}/r_{30}$  ratios than clusters poor in blue galaxies (open dots). Even if the two most distant clusters have both a  $r_{\eta=2}/r_{30}$  ratio larger than the average, there is no convincing statistical evidence for a trend of an increasing  $r_{\eta=2}/r_{30}$  ratio with redshift.

### 4.2. $L_x$ vs $z$

Figure 8 shows that in the BO sample there is a deficit of distant clusters with a x-ray luminosity comparable to faint present-day cluster, and an excess of clusters which are as bright as, or brighter than, the brightest nearby clusters. This holds for the HQ sample as well as for the whole sample. The x-ray luminosity is correlated with  $z$  at the 99.9 % confidence level, according to the Spearman's  $r_s$  and Kendall's  $\tau$  tests. The x-ray luminosity of the four clusters not present in the HQ sample has been converted to our energy band as described in Section 3.5. In the whole sample, clusters rich in blue galaxies (solid dots) are not preferentially the brightest or the faintest ones. The correlation between x-ray luminosity and redshift is still present if we use  $r_{30}$  or a 3 Mpc aperture for all clusters. If we remove the irregular clusters identified by Butcher & Oemler (1984) from the sample the correlation is still present, but only at 98.5 % confidence level.

In the x-ray waveband, distant clusters are not brighter in the past than today, and, if anything, they were fainter in the past, not brighter (Henry et al. 1992; Collins 1997; Vikhlinin et al. 1998; Rosati, Della Ceca, Norman et al. 1998). On the other hand, the x-ray luminosity of the clusters in the BO sample, that span the same redshift and luminosity range of the above-mentioned *representative* samples, increases with redshift (or low luminosity clusters are missing at large  $z$  in the sample). This means that the BO sample is not representative of a homogeneous class of clusters of galaxies observed at different look-back times, but it is biased toward an increasing fraction of bright x-ray clusters as the redshift increases. We postpone the discussion of the relevance of the trend in the BO effect to the next section.

The existence of a strong correlation between x-ray luminosity and redshift, in the BO sample, makes suspicious any other correlation involving these two quantities.

### 4.3. Richness vs $z$

In hierarchical scenarios, clusters at high redshift are more massive, on average, than nearby clusters, since only richest clusters are already formed. Instead, the ancestors of present-day clusters were less massive than today and they had not yet formed at high redshift. Therefore, it is expected that, at higher redshift, clusters (which have already formed) are richer than nearby ones.

Figure 9 shows that the distant clusters in our sample are also the ones with higher ACO richness. The Spearman  $r_s$  and Kendall's  $\tau$  tests reject ( $> 99.9\%$  confidence level) that the richness is not correlated with  $z$ . Dressler et al. (1997), in their study of the morphological segregation in clusters at  $z \sim 0.4$  (half of these taken from the BO list), noted that the distant clusters are denser than nearby ones listed in Dressler (1980).

The increase of the cluster richness with redshift in our (BO) sample is not due to the evolution of clusters, but just to two selection effects: both richness and x-ray luminosity (see Figure 10), and x-ray luminosity and redshift (see Figure 8) are correlated. The latter correlation is certainly a bias, and this induces a correlation between redshift and richness. Therefore the trend between richness and redshift is not a property of the clusters but a result of the (poorly known) selection criteria adopted for assembling the sample.

The (apparent) evolution of the cluster richness is easy to understand from an observational point of view. In the optical, clusters are usually detected as galaxy overdensity over the field. As the redshift increases, the clusters have to be richer and richer to be detected, and distant poor clusters are likely to be missing in all optically selected catalogs. The ACO catalog, on which the Butcher-Oemler sample is largely based (note also that Cl 0939+47 is listed in the ACO catalog as Abell 851), is complete up to  $z \sim 0.1$  (Scaramella et al. 1991). At larger redshifts only the richest clusters are present, whereas at small redshift the number of very rich clusters is small because of the small local volume.

The right panel of Figure 9 shows that the central richness,  $N_{30}$ , of clusters with PSPC data does not increase with redshift, contrary to that expected from its correlation with x-ray luminosity (Figure 10) and from the increase of the x-ray luminosity with  $z$  (Figure 8). However, it is quite dangerous to do predictions by propagating correlations between quantities, especially in a biased sample such as our, since too many properties are changing at the same time as the redshift varies.

$N_{30}$  and  $R$  do not show any statistically significant correlation (the Spearman test indicate a correlation at  $60\%$  confidence level). Poor clusters, in the ACO sense, do not have too many galaxies within  $R_{30}$ , whereas rich clusters can be very rich, as well as very poor, in the center. This means that clusters have a variety of galaxy density profiles for a given  $N_{30}$  or  $R$ , since for the same total number of bright galaxies,  $R$ , they can have quite different central number of galaxies,  $N_{30}$  (and vice versa). Alternatively, large observational errors affect these two quantities.

#### 4.4. $L_x$ vs richness

Figure 10 shows that in the whole sample the cluster x-ray luminosity increases with galaxy richness, as measured by either Abell, Corwin & Olowin (1989) or Butcher & Oemler (1984). Clusters which are rich in blue galaxies (solid dots) span the entire range explored in richness and luminosity. The correlation between x-ray luminosity and cluster richness is expected (e.g. Bahcall 1974; Jones & Forman 1978). However, in our sample, this correlation is probably the result of two selection effects: as the redshift increases, we sample (i) brighter (see Figure 8) and

(ii) richer (Figure 9, left panel) clusters. Our statement can be checked using the data from Smail et al. (1998), who studied very bright x-ray selected clusters, independently from their optical richness. Their clusters have  $\log L_x \sim 45$ ,  $0 < R < 3$  and  $15 < N_{30} < 60$ . Adding these data to ours, the correlation between richness and x-ray luminosity largely disappears, thus confirming that the found correlation is the result of the selection criteria instead of a real clusters property (Figure 11).

#### 4.5. $L_x$ vs $f_b$

A correlation between  $L_x$  and  $f_b$  would explain many cluster properties. The lack of blue galaxies in the cluster core, the color distribution of spiral galaxies and many of their properties, such as velocity and position relative to the cluster center, higher surface brightness (Andreon 1996) and HI deficiency of infalling spirals (Gavazzi 1987) can be explained if spirals falling in clusters have a starburst due to the ram pressure in the hot gas (Bothun & Dressler 1986) that consumes the galaxy's gas reservoir. During the burst, these galaxies become bluer and brighter in the mean surface brightness. Just after the burst, they become as red as ellipticals (Charlot & Silk 1994), explaining the presence of red spirals in cluster cores. Furthermore, both the existence of galaxies that show spectral signatures consistent with the presence of intermediate age stellar populations (Couch & Sharples 1987, Lavery & Henry 1988, Dressler & Gunn 1992), and the photometric evidence for the blue starburst spirals in Coma (Donas et al. 1995, Andreon 1996), give support to this scenario.

We do not observe any correlation between x-ray luminosity and the fraction of blue galaxies for the whole sample and for the HQ sample. In a sample of 10 clusters at moderate redshift ( $z \sim 0.25$ ), which span just a factor 2-3 in x-ray luminosity, a wide spread is found in the fraction of blue galaxies (Smail et al. 1998), which is uncorrelated to x-ray luminosity. Using *Einstein Observatory* data, Lea & Henry (1988) suggest the possible existence of a correlation between these two quantities in a sub-sample of the BO list, provided that deviant points (low luminosity clusters and the most distant cluster) are discarded. The absence of a correlation between the fraction of blue galaxies and the cluster x-ray luminosity implies that this link, if exist, is complex and needs more physical parameters to be explained than only the spiral fraction and the x-ray luminosity.

Here we note that these quantities are not averaged on the same cluster area, nor on regions whose area ratio is fixed: sometimes the optical radius is 3 time larger than the area over which the spiral fraction has been computed, and sometimes it is two times smaller (see Figure 7). For this reasons, we have recalculated the cluster x-ray luminosities within the radius  $r_{30}$  used for computing the cluster spiral fraction, but still any significant correlation between these two quantities does not appear.

#### 5. RELEVANCE OF THESE TRENDS IN THE CONTEXT OF THE BO EFFECT

Any sample of local and distant clusters that is not statistically complete can be affected by the selection criteria adopted to assemble it. This happens because clusters have (i) morphological differences in the nearby universe

(Zwicky 1957) and at  $z \sim 0.4$  (Oemler et al. 1998) and (ii) their galaxy populations are subjected to several segregation effects, both in galaxy morphology (Hubble & Humanson 1922; Dressler 1980; Sanromà & Salvador-Solé 1991; Whitmore, Gilmore & Jones 1993; Andreon 1994, 1996; Dressler et al. 1997; Andreon, Davoust & Heim 1997), color (Butcher, & Oemler 1984; Mellier, Soucail, Fort et al. 1988; Donas et al. 1995; Andreon 1996), and spectral properties (Biviano et al. 1997 and reference therein).

In particular, any selection done on the basis of the richness is contaminated by several factors, such as our ignorance on the physical evolution of the cluster richness or the role played by local phenomena as the enhancement in brightness due to starburst activity. In this sense, selecting clusters according to their x-ray luminosity is safer, because the physics of the x-ray emission is well known, and easier in detecting (the x-ray emission goes as the square of the density, instead of the density for optical richness). Once a sample of clusters is properly defined, the assumption done is that the same class of objects are compared at different look-back times.

*Our results show that the main cluster sample studied up to now in the context of the BO effect is biased:* the x-ray luminosity of these clusters increases with the redshift, contrary to the recent observational evidence for representative samples (see Sect. 4.2). Thus, the nearby and distant clusters in the BO sample are not representative of a fair sample. This implies that any trend highlighted in the BO sample could be the product of the selection criteria adopted instead of real differences with respect to the age of the systems.

Differences in x-ray luminosity reflect, at large extent, differences in the intracluster gas temperature and gas density and, consequently, in the cluster mass (Quintana & Melnick 1982, Edge & Steward 1991, White et al. 1997). Oemler et al. (1997) supposed that they were studying richer and richer clusters as the redshift increases, and that distant clusters were growing in a way different from present-day clusters, i.e. merging smaller clumps at higher rate, as hierarchical scenarios suggest (Kauffmann 1995). This conclusion supposes a physical evolution of the clusters in the BO sample, whereas instead the richness of the clusters in the BO list increases just because of selection effects.

Another piece of evidence for the presence of a selection bias in the BO sample comes from the fact that the BO effect is only evident in optically selected cluster samples. In fact, clusters selected in the x-ray band, with almost the same x-ray luminosity and  $z \sim 0.25$ , show blue fraction values with a large range, and with a mean similar to that observed in nearby clusters (Smail et al. 1998). This mean value is also smaller than the blue fraction in the BO clusters at the same redshift.

To summarize, the BO sample does not contain the same class of objects at different look-back times, contrary to the requirement to detect any sign of evolution in a sample.

We note that, although this bias affects the BO sample, it could not lower the significance of the BO effect, if x-ray bright clusters have the same blue fraction of much fainter clusters. This is a hypothesis that, at the present time, we cannot test observationally on an unbiased sample. In

the BO biased sample, the fraction of blue galaxies does not seem to depend on the x-ray cluster properties. Furthermore, the BO effect is evident even after removing the faint clusters with  $\log(L_X) < 44$  and  $z < 0.1$ . However, we do not know if this reduced sample (or any other subsample drawn from the BO sample) is representative for the range of redshift studied, and any conclusion drawn from it should be regarded with caution. In conclusion, we do not believe that selection biases are completely removed by eliminating offending clusters.

From the theoretical point of view, Kauffmann (1995) shows that in their model of cluster formation and evolution the fraction of blue galaxies does not depend on the cluster mass, at least for rich clusters. In that case, there is no risk in comparing clusters of different masses (x-ray luminosities) at different redshift for studying the BO effect. We stress, however, that the evolutionary interpretation of the BO effect still holds only under the hypothesis that these selection biases do not affect the sample, hypothesis which must be shown to be true.

Galaxies in groups do not show the BO effect (Allington-Smith et al. 1993) over the same redshift range. For this reason, and under the assumption of the evolutionary interpretation of the BO effect in clusters, Allington-Smith et al. (1993) claim that evolution is driven by environment, much more than look-back time. However, selection criteria of studied groups and clusters are quite different: groups are *not* optically selected, because Allington-Smith et al. (1993) built their group sample selecting the galaxies around radio-galaxies of a given radio flux, which is likely to be uncorrelated with the optical luminosity of the galaxy hosting the radio-source, or to the group optical properties. Instead, the BO cluster sample is biased toward very rich (and x-ray luminous) clusters at high redshift. We think that the claim of a differential evolution of galaxies in clusters compared to those in groups, should be pending on a proper determination of the amplitude of the BO effect in a sample of clusters representative of their redshift.

## 6. CONCLUSIONS

We have analysed *Rosat* PSPC images of most of the clusters studied in relation to the Butcher-Oemler effect. We have computed surface brightness profiles, as well as x-ray fluxes within metric diameters adapted to the cluster size (Table 3). Our main results are:

1) The cluster x-ray size, as measured by the Petrosian  $r_{\eta=2}$  radius, does not evolve and it is independent of x-ray luminosity:  $\log r_{\eta=2} \sim 3.10 \pm 0.14$  kpc.

2) The x-ray luminosity of clusters listed in the Butcher-Oemler sample increases with redshift (Figure 8). In the same redshift range, there is observational evidence, from *representative* samples, that the x-ray luminosity of clusters is constant or decreasing i.e. have a trend opposite to those observed in BO sample. Therefore, nearby and distant clusters in the BO sample are not representative of a given class of objects observed at different epochs, and thus the BO sample does not contain the same class of objects at different look-back times, contrary to the requirement to detect any sign of evolution in a sample.

Because selection criteria modify the sample composition in a redshift dependent way, it is quite difficult to

disentangle a real redshift dependence (evolution) from a fictitious redshift trend induced by selection criteria. Hence, the observed BO effect measured from optical selected samples is *not necessarily* a general property of clusters of galaxies, but could be a selection effect. There is some independent support to this interpretation: it seems that x-ray selected clusters, all of similar x-ray luminosity and therefore likely to belong to the same class, do not show the BO effect (Smail et al. 1998). Similarly, galaxies in radio-selected groups show no evolution, beside passive one (Allington-Smith et al. 1993).

The variety of optical shapes and sizes of clusters, together with the Malmquist-like bias and the incompleteness of the BO list, are the main sources for the trends present in the sample.

X-ray data have been of fundamental importance in revealing the existence of a selection bias that mimic the trend usually interpreted as evidence of evolution. It is not surprising, therefore, that our conclusions differ from those reached when x-ray data were not available.

3) The ACO richness of clusters listed in the Butcher-Oemler sample increases with redshift. We interpret this correlation as an observational effect: poor clusters are

scarcely detected at high redshift, and, unusually, rich cluster are missing in low redshift samples. Other cluster quantities ( $N_{30}$ ,  $L_X$ , etc.) shows some correlation among them or with redshift. We explain these as the effect of selection criteria. Adding to our sample a sample of x-ray selected clusters, the correlations generally lose strength, suggesting the correctness of our interpretation.

4) The usual interpretation of the BO effect, as due to evolution, holds only assuming that selection effects have not practical relevance, an hypothesis which must be tested. The absence of correlation between the fraction of blue galaxies and the x-ray luminosity of the clusters may suggest such a possibility.

We are grateful to Sabrina de Grandi for her support and availability at the beginning of this work and to David White and Gilles Theureau for their suggestions on the manuscript. Constructive comments by D. Burstein, G. Bothun and an anonymous referee improved this paper. S.E. acknowledges M. Capaccioli for the financial support of the publication charges of this paper. S.A. dedicates this work to his grand father, Ismaele Andreon, recently deceased.

## REFERENCES

- Abell G., Corwin H., Olowin R., 1989, ApJS 70, 1  
 Allen S., Fabian A., 1998, MNRAS 297, L57  
 Allington-Smith J., Ellis R., Zirbel E., Oemler A., 1993, ApJ 404, 521  
 Andreon S., 1994, A&A 284, 801  
 Andreon S., 1996, A&A 314, 763  
 Andreon S., Davoust E., Heim, A&A, 1997, 323, 337  
 Bahcall N., 1974, ApJ 193, 529  
 Beers T.C., Gebhardt K., Huchra J.P., Forman W., Jones C., Bothun G.D., 1992, ApJ 400, 410  
 Biviano A., Katgert P., Mazure A., 1997, A&A 321, 84  
 Bothun G., Dressler A., 1986, ApJ 301, 57  
 Briel U., Henry J., Boeringer H., 1992, A&A 259, L31  
 Buote D., Canizares C., 1996, ApJ 457, 565  
 Butcher H., Oemler A., 1977, ApJ 219, 18  
 Butcher H., Oemler A., 1984, ApJ 285, 426  
 Cavaliere A., Fusco-Femiano R., 1976, A&A 19, 137  
 Charlot S., Silk J., 1994, ApJ 432, 453  
 Cirimele G., Nesci R., Trevese D., 1997, ApJ 475, 11  
 Collins C., Burke D., Romer A., Sharples R., Nicol R., 1997, ApJ 479, L117  
 Couch W., Sharples R. 1987, MNRAS 229, 423  
 David L., Jones C., Forman W., 1996, ApJ 473, 692  
 Donas J., Milliard B., Laget M., 1995, A&A, 303, 661  
 Dressler A., 1980, ApJ 236, 351  
 Dressler A., Gunn J. 1992, ApJS 78, 1  
 Dressler A., Oemler A., Couch W., et al. 1997, ApJ 490, 577  
 Edge A. & Stewart G. 1991, MNRAS 252, 428  
 Ellis R., 1997, ARA&A 35, 389  
 Ellis R., Colless M., Broadhurst T., Heyl J., Glazebrook, K., 1996, MNRAS 280, 235  
 Ellis R., Smail I., Dressler A., et al. 1997, ApJ 483, 582  
 Evrard A., 1990, ApJ 363, 349  
 Evrard A., 1991, MNRAS, 248, 88  
 Gavazzi G., 1987, ApJ 320, 96  
 Gunn J., Gott J., 1972, ApJ 176, 1  
 Jones C., Forman W., 1978, ApJ 224, 1  
 Jones L., Scharf, C., Ebeling, H., Perlman, E., Wegner, G., Malkan, M., & Horner, D., 1998, ApJ, 495, 100  
 Henry J., Branduardi G., Fabricant D. et al., 1979, ApJ 234, L15  
 Henry J., Gioia I., Maccacaro T. et al., 1992, ApJ 386, 408  
 Huang J.-S., Cowie L., Luppino G., 1998, ApJ 463, 31  
 Hubble E., Humason M., 1926, ApJ 64, 321  
 Kauffmann G., 1995, MNRAS 274, 161  
 Lavery R., Henry J.P., 1988, ApJ 330, 596  
 Lea S.M., Henry J.P., 1988, ApJ 332, 81  
 Lilly S., Tresse L., Hammer F., Crampton D., LeFevre O., 1995, ApJ 455, L8  
 Maccacaro T., Gioia I., Zamorani G. et al. 1982, ApJ 253, 504  
 Markevitch M., Vikhlinin A., 1997, ApJ 491, 467  
 Mellier Y., Soucail G., Fort B., Mathez G., 1988, A&A 199, 13  
 Morrison R., McCammon D., 1983, ApJ, 270, 119  
 Mushotzky R., Scharf C., 1997, ApJ 482, 13  
 Koo D., 1981, ApJ 251, L75  
 Oemler A., Dressler A., Butcher H., 1997, ApJ 474, 561  
 Petrosian V., 1976, ApJ 209, L1  
 Quintana H., Melnick J. 1982, AJ 87, 972  
 Raymond J.C., Smith B.W., 1977, ApJS, 35, 419  
 Rosati P., Della Ceca R., Norman C., Giacconi R., 1998, ApJ 492, L21  
 Sadat R., Blanchard A., Guiderdoni B., Silk J., 1998, A&A 331, L69  
 Sandage A., 1988, ARA&A 26, 561  
 Sandage A., Perelmuter J.-M., 1990, ApJ 350, 481  
 Sanromà M., Salvador-Solé E., 1990, ApJ 360, 16  
 Scaramella R., Zamorani G., Vettolani G., Chincarini G., 1991, AJ 101, 342  
 Schindler S., Prieto M., 1997, A&A 327, 37  
 Schindler S., Wambsganss J., 1996, A&A 313, 113  
 Smail I., Edge A., Ellis R., Blandford R., 1998, MNRAS, 293, 124  
 Soltan A., Henry J., 1983, ApJ 271, 442  
 Stanford S., Eisenhardt P., Dickinson M., 1995, ApJ 450, 512  
 Stanford S., Eisenhardt P., Dickinson M., 1998, ApJ 492, 461  
 Stark A., Gammie C., Wilson R., et al., 1992, ApJS 79, 77  
 Vikhlinin A., McNamara B., Forman W., Jones C., Quintana H., 1998, ApJ, 498, L21  
 de Vaucouleurs G., 1976  
 Wang Q., Ulmer M., 1997, MNRAS, 292, 920  
 White D.A., Jones C., Forman W., 1997, MNRAS 292, 419  
 Whitmore B., Gilmore D., Jones C., 1993, ApJ 407, 489  
 Zwicky F., 1957, Morphological Astronomy, Springer-Verlag

TABLE 1  
THE BO SAMPLE

name	$z$	$r_{30}$ arcmin	$N_{30}$	$f_b$	nh [ $10^{20}$ atoms $\text{cm}^{-2}$ ]	R	X-ray?
Virgo	0.0033	120	21	0.04	...	...	✓
Abell 262	0.0164	27	22	0.02	5.3	0	✓✓
Abell 1367	0.02	25	20	0.4	2.1	2	✓✓
Abell 400	0.0232	17	30	0.05	8.7	1	✓✓
Abell 1656	0.0232	22	94	0.03	0.91	2	✓✓
Abell 2199	0.0305	18	94	0.04	0.88	2	✓✓
Abell 2634	0.0322	30	60	0.02	4.9	1	✓✓
Abell 2151	0.0371	14	29	0.14	3.4	1	✓✓
Abell 2256	0.0581	11	116	0.03	4.2	2	✓✓
Abell 1904	0.0714	9.4	68	0.02	1.8	2	✓✓
Abell 401	0.0748	10.7	92	0.02	1.1	2	✓✓
Abell 2670	0.0749	4.9	51	0.04	2.7	3	✓✓
Cl 0004.8-34	0.114	5.9	60	0.07	...	...	...
Abell 2218	0.171	5.8	114	0.11	3.3	4	✓✓
Abell 1689	0.1747	5.8	124	0.09	1.8	4	✓✓
Abell 520	0.203	4.5	126	0.07	7.6	3	✓✓
Abell 963	0.206	3.6	88	0.19	1.4	0	✓✓
Abell 223	0.207	3.2	67	0.10	1.9	3	✓✓
Abell 222	0.211	1.6	45	0.06	1.8	3	✓✓
Abell 1963	0.221	1.5	38	0.10	...	2	...
Abell 1942	0.224	2.8	57	0.17	...	3	✓
Abell 2397	0.224	2.0	23	-0.04	5.6	3	✓✓
Abell 777	0.226	1.4	15	0.05	1.9	4	✓✓
Abell 2111	0.229	4.1	155	0.16	1.9	3	✓✓
Abell 1961	0.232	3.4	88	0.10	...	3	...
Abell 2645	0.246	1.4	35	0.03	...	4	✓
Abell 2125	0.2472	2.3	62	0.19	2.9	4	✓✓
Abell 1758	0.280	2.4	91	0.09	1.1	3	✓✓
Cl 1446+26	0.369	0.9	42	0.36	...	...	...
Abell 370	0.373	2.2	107	0.21	...	2	✓
Cl 0024+16	0.39	1.1	87	0.16	4.2	2	✓✓
Cl 0939+47	0.407	1.0	...	0.4	1.3	5	✓✓
3C295	0.465	1.0	45	0.22	...	...	✓
Cl 0016+16	0.541	1.0	65	0.02	4.1	4	✓✓



TABLE 2  
DATASET ID, EXPOSURE TIME, ADOPTED CENTERS, AXIS RATIOS AND PA FOR THE STUDIED CLUSTERS

name	ID	$t_{exp}$ <sup>a</sup> sec	center J2000	$b/a$	PA <sup>b</sup>
Abell 262	rp800254n00	8163	1 52 47 +36 09 22	0.87	45
Abell 1367	rp800153n00	17610	11 44 49 +19 41 28	1	0
Abell 400	rp800226n00	22203	2 57 35 + 6 00 25	0.66	30
Abell 1656	rp800005n00	19819	12 59 42 +27 56 34	1	0
Abell 2199	rp800644n00	38244	16 28 38 +39 32 52	0.76	135
	rp150083n00	10063	16 28 39 +39 33 07	0.76	135
Abell 2634	rp800014a01	9826	23 38 29 +27 01 55	1	0
Abell 2151	rp800517n00	11341	16 04 36 +17 43 21	1	0
Abell 2256	rp100110n00	16452	17 03 54 +78 38 19	1	0
Abell 1904	rp800257n00	3627	14 22 16 +48 30 58	1	0
Abell 401	rp800182n00	6289	2 58 59 +13 34 35	0.6	30
	rp800235n00	7009	2 58 59 +13 34 40	0.6	30
Abell 2670	rp800420n00	16554	23 54 14 -10 24 53	0.74	45
Abell 2218	rp800097n00	39579	16 35 52 +66 12 34	0.83	0
Abell 1689	rp800248n00	13142	13 11 29 - 1 20 32	1	0
Abell 520	rp800480n00	4565	4 54 10 + 2 55 04	1	0
Abell 963	rp900528n00	9989	10 17 12 +39 02 40	1	0
Abell 223	rp800048n00	6402	1 37 56 -12 49 08	1	0
Abell 222	rp800048n00	6402	1 37 34 -12 59 23	1	0
Abell 2397	rp800344n00	13629	21 56 09 + 1 23 25	1	0
Abell 777	rp800049n00	7464	9 29 20+78 16 34	1	0
Abell 2111	rp800479n00	7028	15 39 41 +34 24 52	1	0
Abell 2125	rp800511n00	11340	15 41 06 +66 16 13	0.6	135
Abell 1758	rp800047n00	16142	13 32 42 +50 32 54	0.7	135
Cl 0024+16	rp800524n00	1069	0 26 35 +17 09 43	1	0
Cl 0939+47	rp800102n00	13098	9 43 00 +46 59 31	0.74	30
Cl 0016+16	rp800253n00	40325	0 18 34 +16 26 16	1	0

<sup>a</sup>Exposure times are read in the central region of the exposure map.

<sup>b</sup>PAs are from North to East anticlockwise

NOTE.—The two pointing of Abell 2199 (Abell 401) have been acquired 3 years (6 month) apart. Positions listed assumes no pointing errors.

TABLE 3  
RESULTS OF THE ANALYSIS

name	$\log(r_{\eta=2})$ [kpc]	$\log(L(r < r_{\eta=2}))$ [erg s <sup>-1</sup> ]	$\log(L(r < r_{30}))$ [erg s <sup>-1</sup> ]
Abell 262	2.96	43.66	43.64
Abell 1367	3.03	43.86	43.83
Abell 400	3.11	43.47	43.39
Abell 1656	3.10	44.60	44.56
Abell 2199	2.83	44.39	44.41
Abell 2634	3.15	43.78	43.79
Abell 2151	3.33	43.96	43.82
Abell 2256	3.10	44.64	44.62
Abell 1904	3.34	43.86	43.76
Abell 401	3.26	44.80	44.77
Abell 2670	3.03	44.17	44.09
Abell 2218	3.05	44.73	44.75
Abell 1689	2.87	45.08	45.11
Abell 520	3.22	44.90	44.86
Abell 963	3.31	44.82	44.68
Abell 223	3.17	44.47	44.35
Abell 222	3.29	44.49	44.13
Abell 2397	3.12	44.60	44.45
Abell 777	...	~43.86	43.43
Abell 2111	3.24	44.76	44.71
Abell 2125	3.08	44.22	44.14
Abell 1758	3.10	45.00	44.94
Cl 0024+16	...	~44.37	44.25
Cl 0939+47	3.08	44.95	44.41
Cl 0016+16	3.05	45.25	45.07

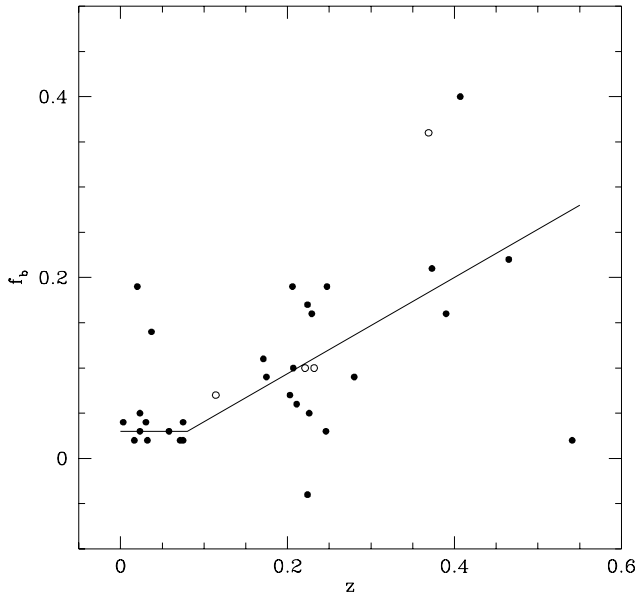
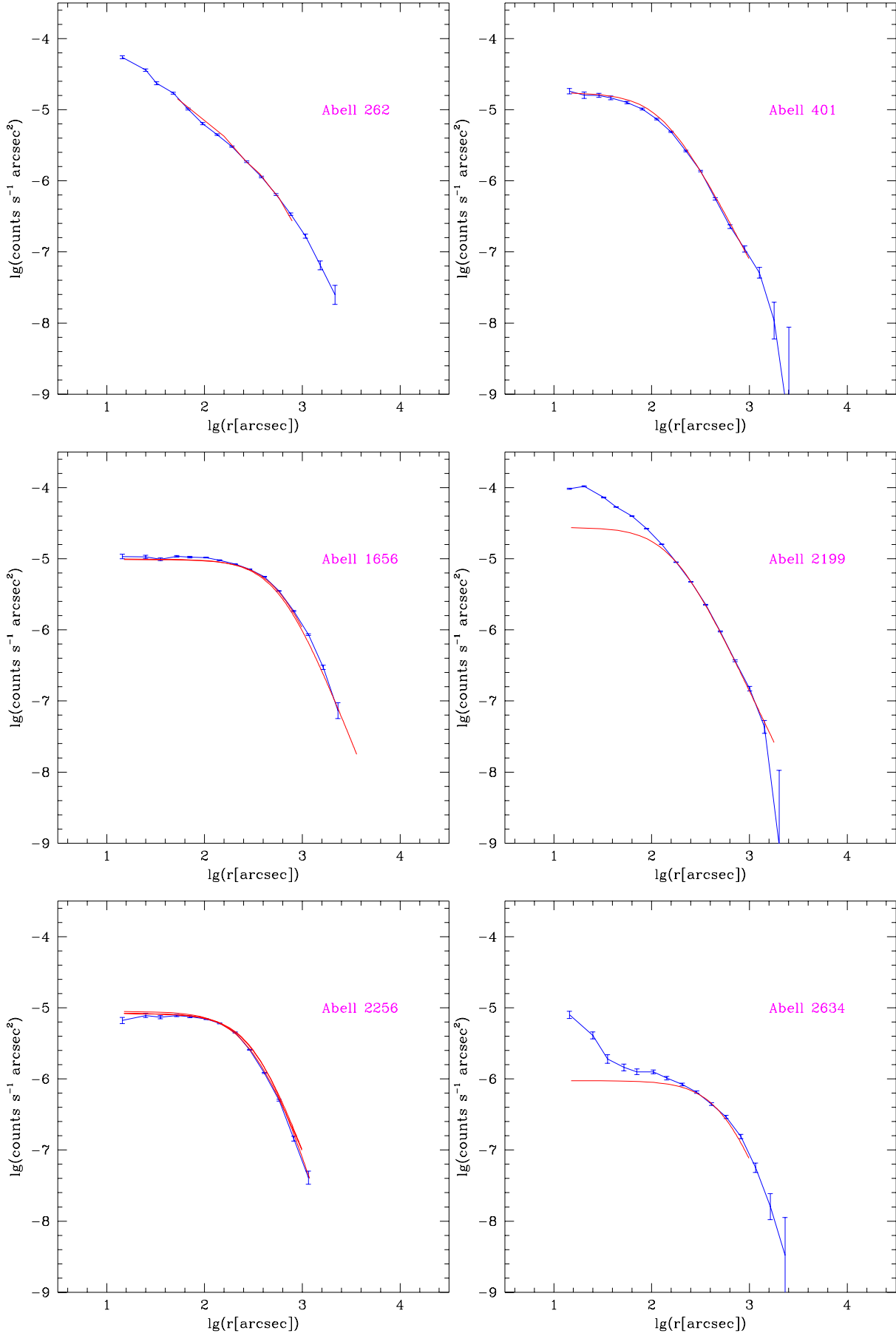


FIG. 1.— Blue fraction as a function of  $z$  for the whole sample (which is the BO sample with the addition of the cluster C1 0939+47). Close and open points mark clusters with and without x-ray data, respectively. The spline is the Butcher & Oemler (1984) eye fit to the data.



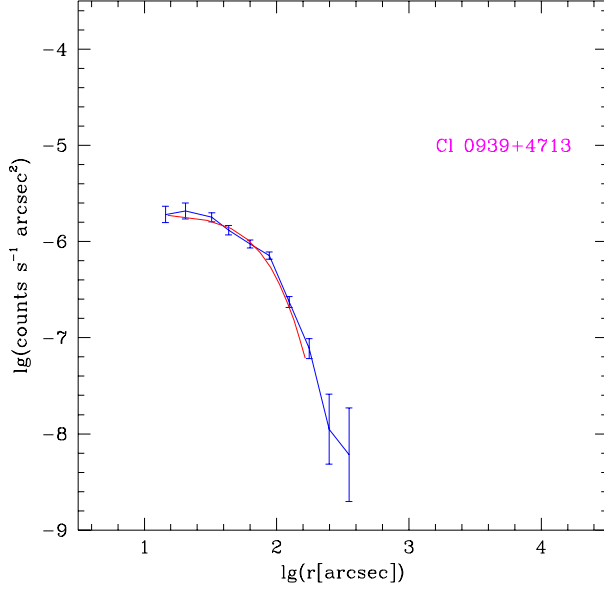


FIG. 2.— Comparison between literature fit and our x-ray profiles

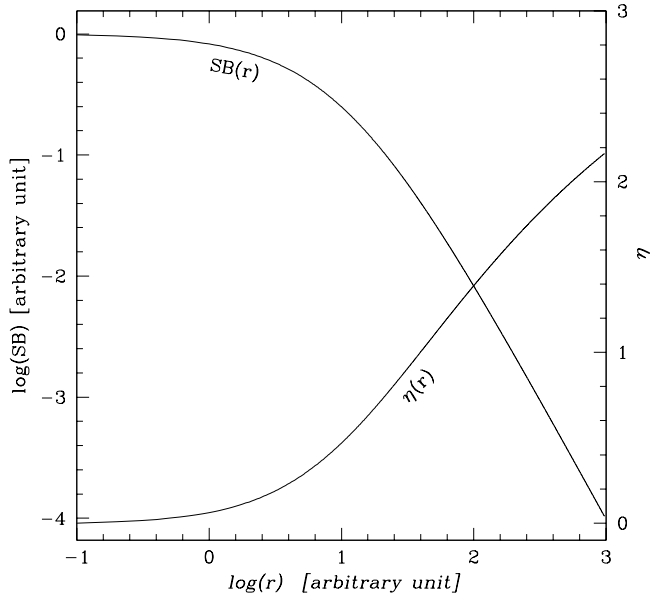


FIG. 3.— SB (Surface Brightness) and  $\eta$  profiles for a King profile with  $\beta = 0.5$  and arbitrary core radius and central surface brightness

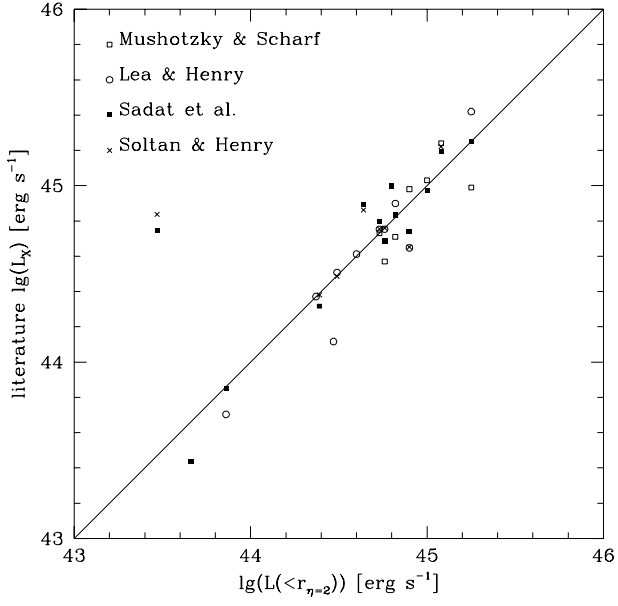


FIG. 4.— Comparison between our metric fluxes in the *Rosat* hard band and isophotal or aperture fluxes from older satellites converted in our system.

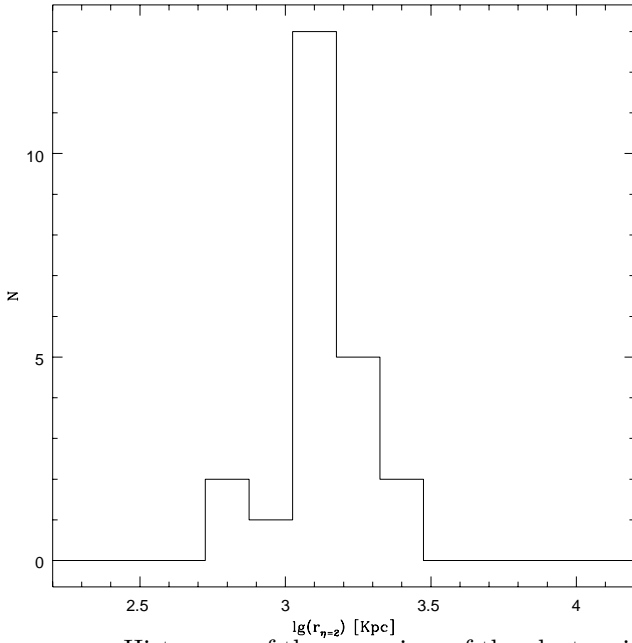


FIG. 5.— Histogram of the  $r_{\eta=2}$  sizes of the clusters in the HQ sample.

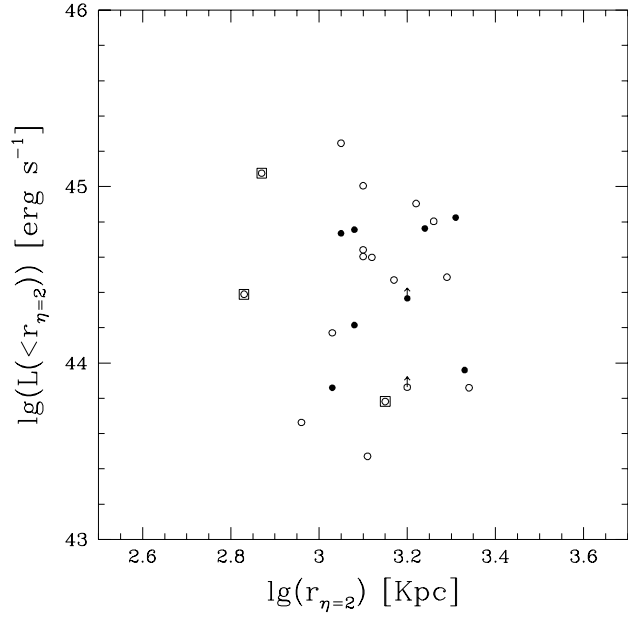


FIG. 6.— X-ray cluster luminosity as a function of the size for clusters in the HQ sample. Solid dots are clusters rich in blue galaxies ( $f_b > 0.1$ ), open dots are clusters poor in blue galaxies. Squares are cooling flow clusters.

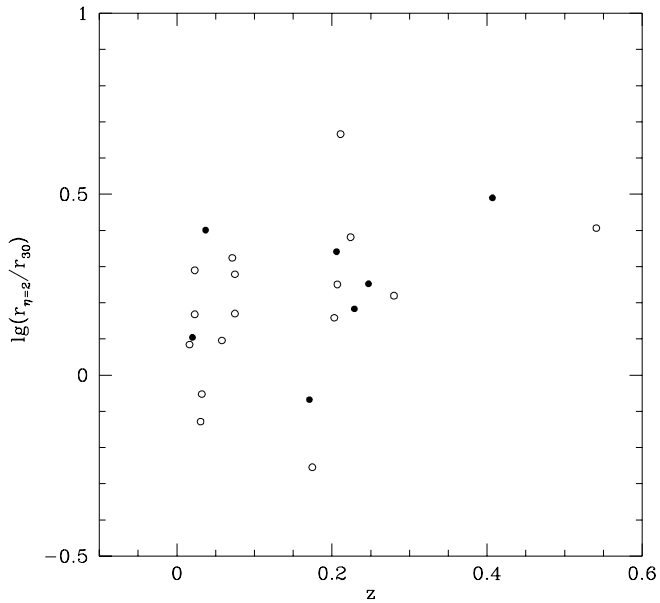


FIG. 7.— Ratio between the optical radius  $r_{30}$  and the x-ray size  $r_{\eta=2}$  as a function of  $z$  for clusters in the HQ sample. Symbols as Figure 6.

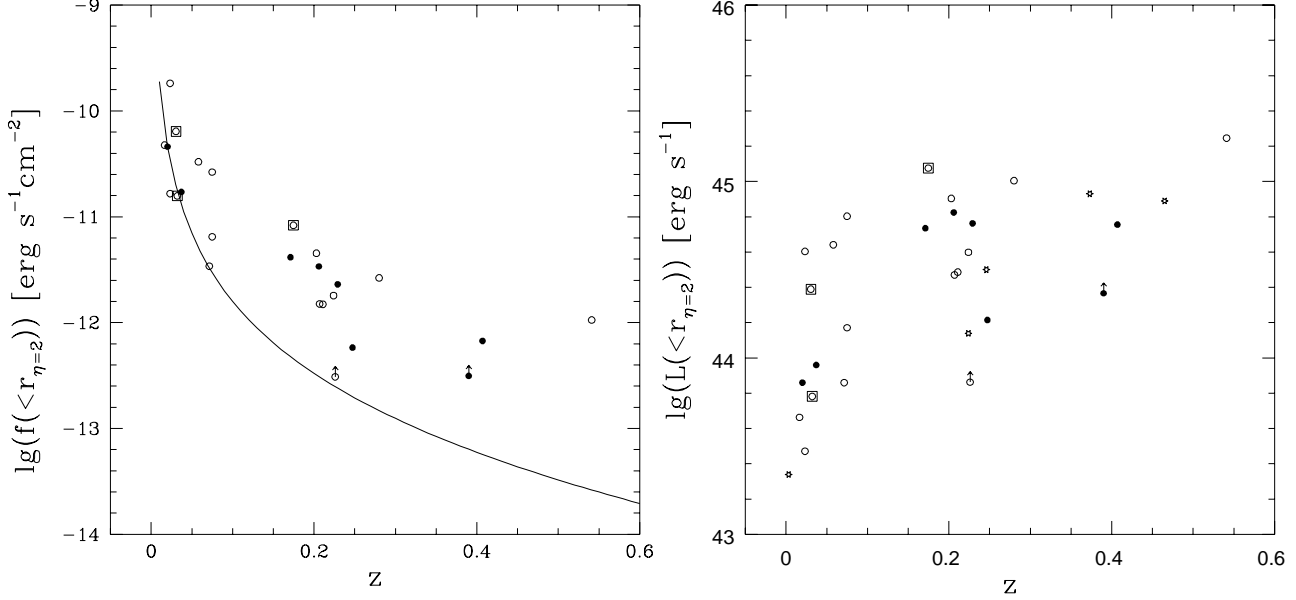


FIG. 8.— X-ray luminosity as a function of  $z$ . Left panel: apparent flux of clusters in the HQ sample. The curve is the locus of the clusters having an x-ray emission 5 time smaller than Abell 1656 (Coma), assuming a K-correction equal to zero. Points are not corrected for absorption or K-correction. Right panel: Absolute luminosity for the whole sample. Absorption and K corrections have been applied to the data. Literature data are plotted as star points. Other symbols as Figure 6.

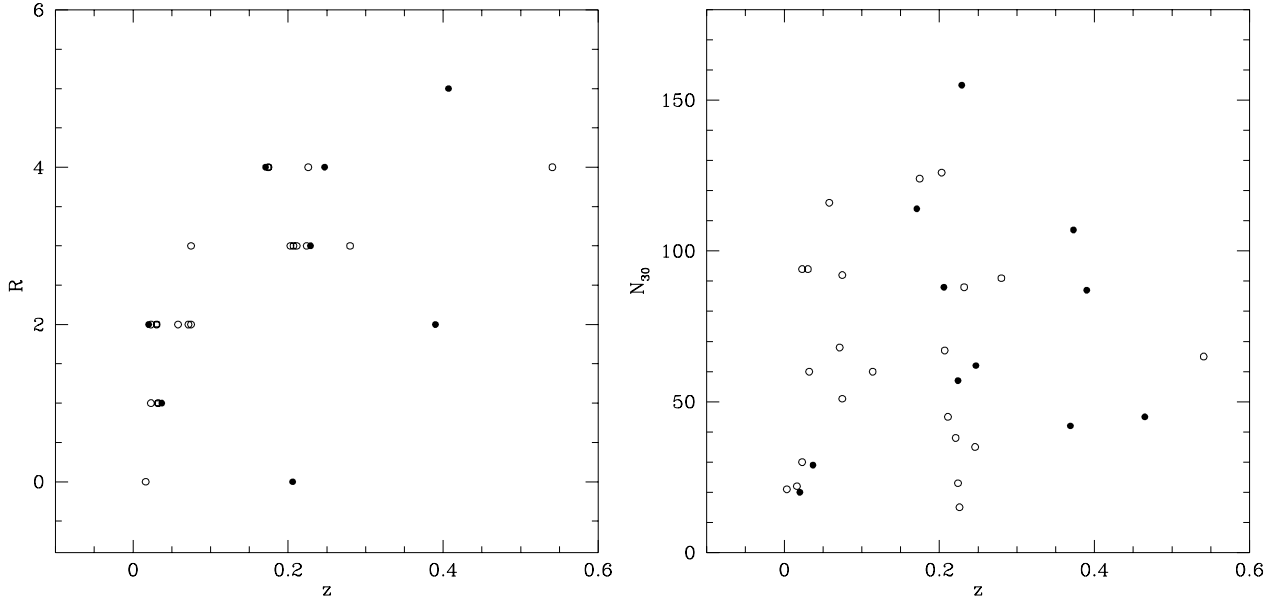


FIG. 9.— Richness as a function of  $z$  for the whole sample. Left panel: ACO richness, right panel: BO richness. Solid dots are clusters rich in blue galaxies ( $f_b > 0.1$ ), open dots are clusters poor in blue galaxies.



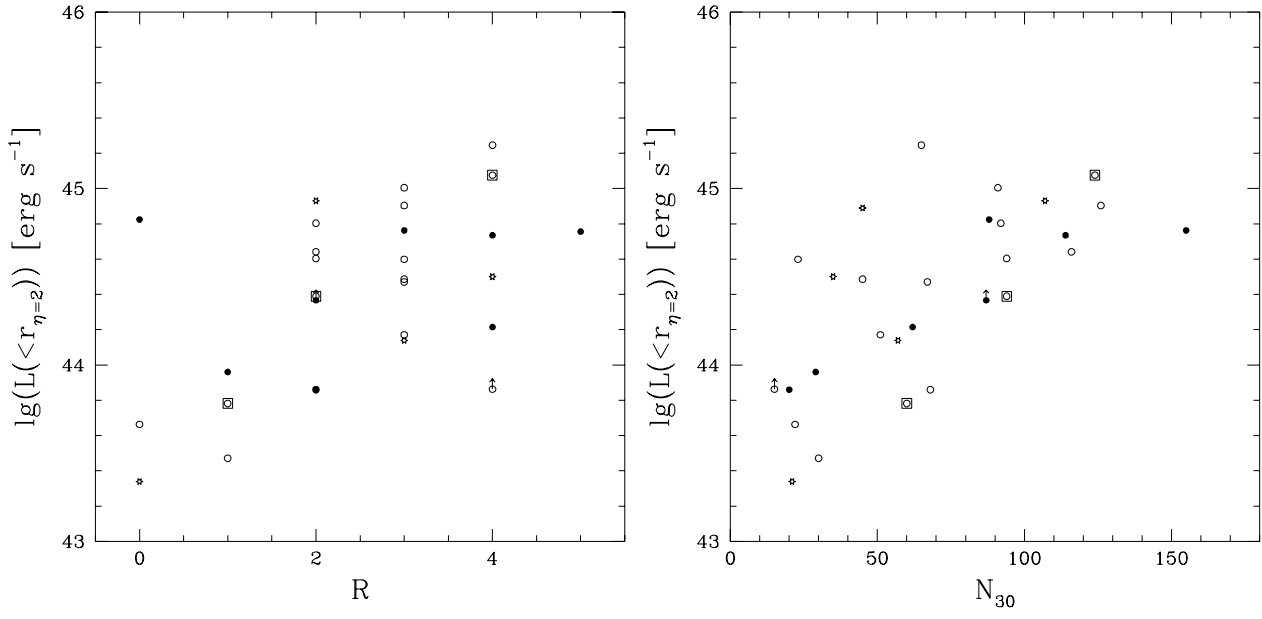


FIG. 10.— X-ray luminosity as a function of the cluster richness for the whole sample. Left panel: ACO richness, right panel BO richness. Symbols as Figure 8.

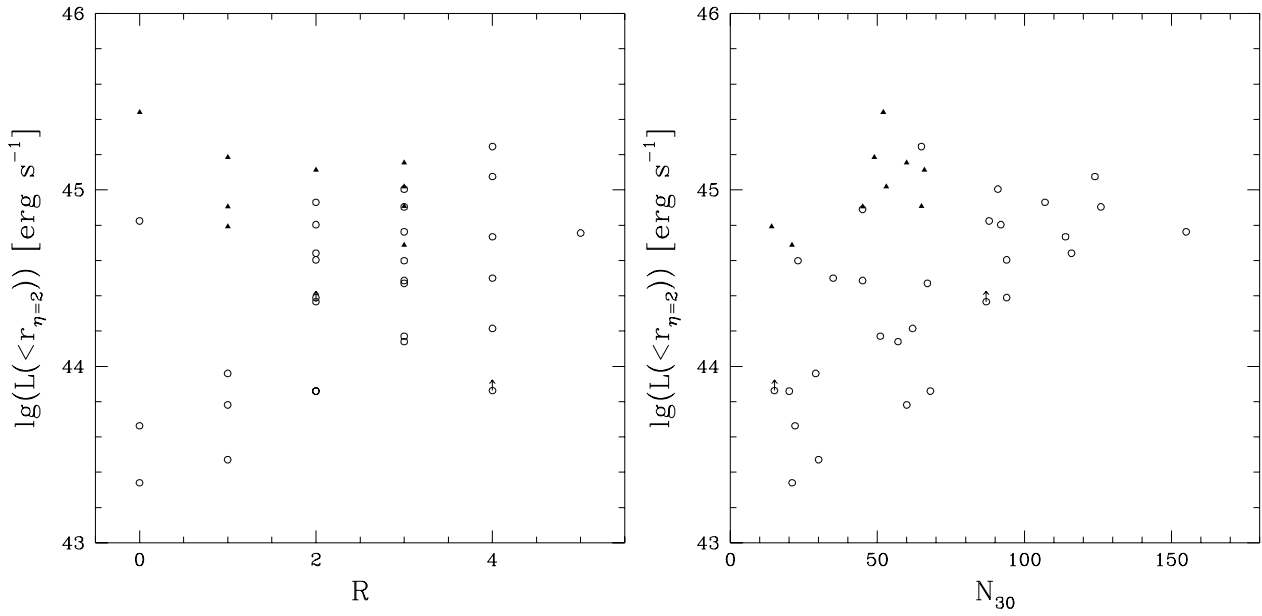


FIG. 11.— X-ray luminosity as a function of the cluster richness, including the Smail et al. (1998) sample. Left panel: ACO richness, right panel BO richness. Open points are the optically-selected BO sample, close triangles are the X-ray selected sample.